DOI: 10.1002/cbic.200800017

Solution Structure of a Functional Biomimetic and Mechanistic Implications for Nickel Superoxide Dismutases

Matthias Schmidt,[b] Stefan Zahn,[c] Michela Carella,[d] Oliver Ohlenschläger,[d] Matthias Görlach,*[d] Erika Kothe,*[e] and James Weston*[a]

*The nickel complex of a synthetic nonapeptide (HCDLPCFVY-NH_2) is capable of catalytically disproportionating $O_2^{\bullet-}$ and is thus a functional biomimetic for nickel superoxide dismutases. This represents a simplification as compared to a NiSOD "maquette" that is based on a dodecapeptide that was recently reported [*Inorg. Chem. ***2006***, 45, 2358]. The 3D solution structure reveals that the first six residues form a stable macrocyclic structure with a preformed binding site for Ni^{II}. Proline 5 exhibits a* trans *peptide linkage in the biomimetic and a* cis *conformation in NiSOD enzymes. DFT calculations reveal the source of this preference. Mechanistic consequences for the mode of action (identity of the fifth ligand) are discussed. The SOD activity is compared to enzymatic systems, and selected modifications allowed the biomimetic to be reduced to a functional minimal motif of only six amino acids (ACAAPC-NH_2).*

Introduction

Respiration produces toxic superoxide anions ($O_2^{\bullet-}$) as a by-product in rather large concentrations. These are believed to play an important role in aging processes as well as in many disorders ranging from inflammatory to neurodegenerative diseases.[1] Nature deals with these reactive oxygen species (ROS) by employing an efficient metallo-based enzymatic protection system, the superoxide dismutases (SOD; EC 1.15.1.1). These metalloenzymes intercept $O_2^{\bullet-}$ and convert it into O_2 and H_2O_2 via a generic two-step, ping-pong redox mechanism [Eqs (1) and (2)]:

$$O_2^{\bullet-} + M^{ox} \rightarrow O_2 + M^{red} \quad (1)$$

$$O_2^{\bullet-} + M^{red} + 2H^+ \rightarrow H_2O_2 + M^{ox} \quad (2)$$

in which M is a transition metal ion that is capable of a reversible one-electron redox reaction. [2]

Until recently, SODs have been considered to contain either a Fe[3,4] or Mn[2,4,5] atom-based mononuclear active site, or to have a binuclear Cu/Zn[2,6] core. In 1996, a new class of nickel-dependent SODs were discovered in *Streptomyces*.[7,8] In the meantime, NiSODs have also been identified in several marine cyanobacteria,[9] and a heavy-metal-resistant strain has been discovered by one of us (Kothe et al.) in the former uranium mines in eastern Germany.[10]

Although the chemical task remains the same, NiSOD amino acid sequences, metal ligand spheres, and general structural features deviate significantly from all other SODs, thus indicating an independent evolutional history.[11] Nevertheless, NiSODs have many mechanistic characteristics in common with other SODs (ping-pong redox mechanism with similar catalytic rate constants, pH dependence, etc.) The gene *sodN* that encodes NiSOD has been identified in several *Streptomyces*[7b,10,11] and cyanobacteria.[9] The initial preprotein that is translated from *sodN* (inactive) is relatively short (about 131 amino acids) and does not contain Ni^{II}.[7b,12] Removal of an N-terminal extension of 14 residues, which is assumed to be performed by a peptidase that has not yet been identified triggers folding into the tertiary structure coincident with the irreversible uptake of Ni^{II} , after which full SOD activity is observed.[7b,12]

Some discussion originally existed as to whether the NiSOD active site is mono- or binuclear.[13] However, two X-ray crystallographic structures [*S. seoulensis* (1.68 Å resolution) and *S. coelicolor* (1.30 Å)] have confirmed a mononuclear active site.[14,15] Both variants possess a hexameric quaternary structure with each subunit containing an active site with a single covalently bound nickel ion. Most intriguing is the fact that the active site is isostructural at least as far as the environment in the imme-

[a] *Prof. Dr. J. Weston*
Departamento de Química, Universidad Nacional de La Plata
47 y 115 C.C. 962–1900 La Plata (Argentina)
Fax: (+54) 221-425-9485 ext. 30
E-mail: jweston@quimica.unlp.edu.ar

[b] *Dr. M. Schmidt*
Leibniz-Institut für Altersforschung
Beutenbergstrasse 11, 07745 Jena (Germany)

[c] *S. Zahn*
Wilhelm-Ostwald-Institut der Universität Leipzig
Linnestrasse 2, 04103 Leipzig (Germany)

[d] *M. Carella, Dr. O. Ohlenschläger, Dr. M. Görlach*
Leibniz Institut für Altersforschung
Beutenbergstrasse 11, 07745 Jena (Germany)
E-mail: mago@fli-leibniz.de

[e] *Prof. Dr. E. Kothe*
Institut für Mikrobiologie der Friedrich-Schiller-Universität
Neugasse 25, 07743 Jena (Germany)
E-mail: erika.kothe@uni-jena.de

Supporting information for this article is available on the WWW under http://www.chembiochem.org or from the author.

diate neighborhood of the nickel ion is concerned. However, distinct differences are observed in the secondary sphere. One of these structures (*S. coelicolor*) possesses a narrow electrostatic guidance channel that is provided by three Lys residues;[14] this is reminiscent of some FeSODs[3] that are suspected to operate by an outer-sphere mechanism in which a direct metal–substrate bond is not involved (fixation of $O_2^{\bullet-}$ in the neighborhood of Ni^{II} with through-space electron transfer from Ni^{II} to substrate).[3,4] The other structure (*S. seoulensis*) provides no evidence for electrostatic guidance,[15] and a previous study demonstrated that k_{cat} does not depend on the ionic strength of the medium;[11a] both facts suggest that an outer-sphere mechanism could be operating in this variant.[15] These findings raise the question of which general mechanism (inner vs. outer sphere) is operating.

Spectroscopic investigations have shown that the metallocenter can easily cycle between diamagnetic Ni^{II} and paramagnetic Ni^{III} states, and that the number of ligands changes as a function of the oxidation state.[13,16] In accord with these findings, the crystal structures contain two different nickel species, a square planar N,N,S,S-coordination geometry for the reduced Ni^{II} form, and a square pyramidal geometry for the Ni^{III} form in which the imidazole ring of His1 is axially coordinated (species **1** and **3** in Scheme 1).[14,15]

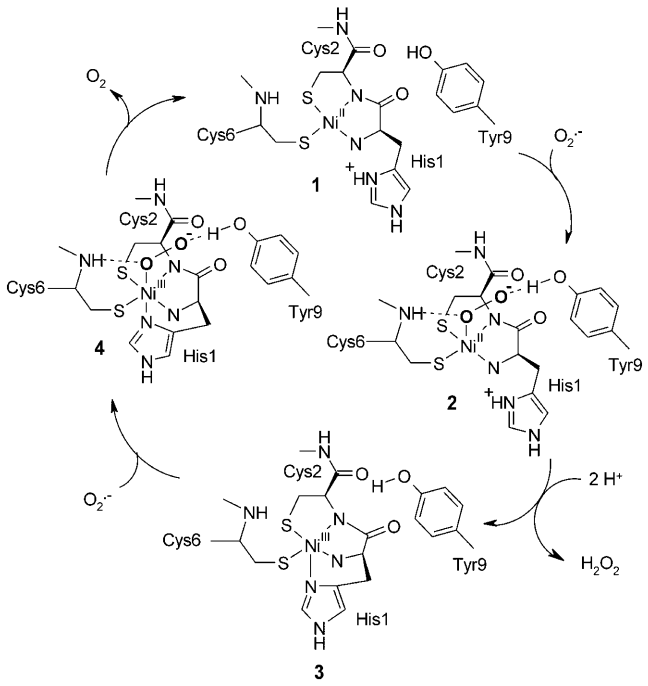

Scheme 1. Postulated mode of action of NiSOD that is based on experimental evidence.

The current understanding of the mode of action of NiSOD is based on experimental data[11–16] and operates on the assumption of an inner-sphere mechanism, which is initiated when $O_2^{\bullet-}$ (after having entered the active site possibly through an electrostatic channel[15]) binds to the vacant axial site of Ni^{II} on the side opposite to the His1 residue. It is possible that Tyr9 moves aside upon approach of $O_2^{\bullet-}$, thus providing a more direct access to the central ion.[17]

It has been postulated that Tyr9 and/or the backbone amide of Cys6 intercepts and appropriately positions $O_2^{\bullet-}$ for a one-electron transfer ($Ni^{II} \rightarrow Ni^{III}$), which is accompanied by double protonation from yet unidentified general acids in the immediate vicinity of the active site.[14]

After H_2O_2 is generated, it is believed to be displaced from the now oxidized active site by His1, which attacks from the back side to form the pentacoordinated oxidized form **3** of NiSOD. In the second half of the catalytic cycle, intermediate **3** accepts a second molecule of $O_2^{\bullet-}$—again this is postulated to be positioned by Tyr9 and Cys6—to form a hexacoordinate intermediate or transition structure **4**. A one-electron transfer in the reverse direction ($Ni^{III} \rightarrow Ni^{II}$) generates molecular O_2, which along with His1 is immediately released from the coordination sphere of the newly generated Ni^{II} ion, which clearly prefers a square planar coordination sphere.

In the meantime, several computational studies have demonstrated that this mode of action is considerably oversimplified.[18–20] A multitude of possible intermediates and mechanisms, which are further complicated by the possibility of various proton sources as well as a variable spin (high or low) on nickel are theoretically possible. For example, one current study suggests that as $O_2^{\bullet-}$ approaches the active site, it is protonated *before* it reaches the central nickel ion. The actual docking species is postulated to be a hydroperoxyl radical ($^{\bullet}OOH$).[18] Another study indicates that end-on coordination of $O_2^{\bullet-}$ to Ni^{II} accompanied by a one-electron transfer from Ni^{II} to $O_2^{\bullet-}$ could be the first step.[19] This would generate two different intermediates: a Ni^{III}–O_2^- superoxide and a Ni^{III}–OOH species (possible proton donor is the backbone amide in Cys6).[19] The proton(s) needed to produce H_2O_2 could originate from several different sources: the side chains of Tyr9, His1, Asp3 residues as well as the backbone amide in Cys6.[19] It is clear that further extensive work both of computational and experimental nature is necessary before a detailed understanding of the individual steps in the catalytic turnover is reached.

It is interesting that a well-conserved sequence of twelve amino acids is found in all known NiSODs.[14] Known as the "nickel hook", most, if not all, of the interactions that are essential for metal binding are provided by this sequence, which folds around the metal ion in a manner that is reminiscent of an organometallic macrocycle[14,15] (Figure 1). In the absence of nickel, the active site is disordered.[14] It is believed that the nickel coordination chemistry controls the local protein conformation.[21]

If an inner-sphere mechanism is the predominate mode of action, the bulk of the enzyme should basically be ballast as far as the chemical reaction is concerned. Although second-sphere effects will most likely modify and/or optimize the activity, this hook should provide a functional biomimetic for NiSODs in general. This was recently confirmed by Shearer and Long, who demonstrated that a nickel complex of this hook sequence (the first twelve residues of *S. coelicolor* NiSOD) pro-

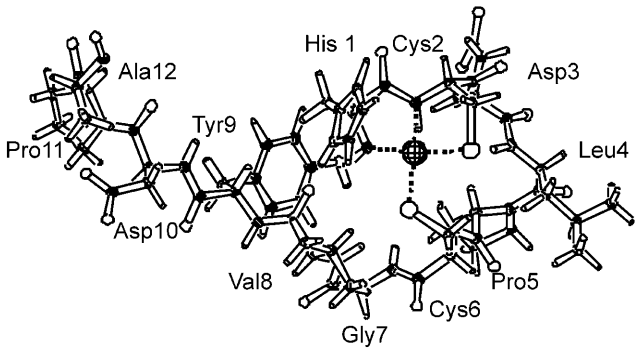

Figure 1. Solid-state structure of the "nickel hook" in NiSOD. PDB file 1Q0M (reference 15).

vides a "maquette" that successfully converts KO_2 into O_2 and H_2O_2, and the sequence has also tested positive for SOD activity according to standard assays.[22]

Because the last three residues simply attach the hook to the bulk of the enzyme, we have now synthesized a nonapeptide sequence (*S. coelicolor*) and complexed it with nickel ions in the hope of obtaining a smaller functional biomimetic Equation (3):

His1-Cys2-Asp3-Leu4-Pro5-Cys6-Gly7-Val8-Tyr9 (3)

We now demonstrate that a nickel complex of this shorter sequence also possesses considerable SOD activity. We have resolved the 3D solution structure of this biomimetic and quantified the activity. Mutational permutations of selected residues have allowed us to identify a minimal functional structural motif. Where possible, we compare our results to the somewhat larger maquette of Shearer and Long as well as other enzymatic systems. Preliminary computational (DFT) results as well as mechanistic implications are also discussed.

Results and Discussion

Characterization of the nonapeptide and its nickel complex

The synthesis of the nonapeptide (HCDLPCGVY-NH_2) was completely unproblematic. It is fairly stable and soluble in water, MeOH, and DMSO. Solutions can be stored in the refrigerator (5 °C) for several days before disulfide bridges form. It is storable for an indefinite period in the solid state at −20 °C. However, the peptide is somewhat hygroscopic and interacts strongly with salts. Most samples contain only 50–60% nonapeptide; this makes reliable quantitative determinations difficult and necessitates mass corrections as obtained by quantitative amino acid analyses (ASA).

Solutions (1:1) of the nonapeptide and Ni^{II} are very light-pink and are fairly stable in water (unbuffered), MeOH, and DMSO, and can be stored under ambient conditions without further care for about one to two days (up to two weeks in the refrigerator). This system is more stable than the maquette of Shearer and Long, which is reported to decompose if exposed to air for several hours.[22] The only difference lies in the additional three residues Asp10-Pro11-Ala12. If these function as an anchor unit, they probably have little else to do but "flutter" around. This might destabilize the 3D structure. It is also quite likely that the Asp10 residue (Asp3 is obviously less sensitive) is detrimental to the stability. Asp has been reported to easily undergo autooxidation in the presence of redox active metals.[23]

Mass spectroscopic experiments (ESI) of unbuffered methanol solutions (water solutions gave poor results in ESI experiments) show a clear preference for a [1:1] complex (Figure S1 in the Supporting Information). However, small amounts of [1:2] Ni^{2+}/peptide species were detected. Ni^{2+} incorporation into the peptide seems to be a rather slow process in unbuffered MeOH solutions; this is probably due to the necessity of deprotonating the thiol groups. ESI measurements on freshly prepared samples show a considerable amount of free peptide, which slowly disappears over the course of one to two days (refrigerator). In addition, it is necessary to add an excess (2 equiv) of Ni^{II} ions in order to obtain spectra without free peptide.

In direct contrast to the ESI spectra (and the system of Shearer and Long), UV/visible titration experiments (0.1 M phosphate buffered aqueous solutions at pH 7.8) indicate that Ni^{II} seems to coordinate to the peptide in a 2:1 ratio (Figure S2). This indicates that either an equilibrium between free peptide and Ni^{II} complex is present and excess Ni^{II} is needed to shift the equilibrium towards the complex, or that an additional Ni^{II}, which is easily lost coordinates loosely (probably to one of the side chains). Perhaps the steric bulk of the "anchor" residues in the 12-mer maquette[22] helps to hinder such equilibria. At Ni^{II} concentrations of greater than 2 equivalents, the titration shows a slight decrease in the complexation ratio; a fact that we attribute to a competition between PO_4^{2-} from the buffer and the peptide for Ni^{II} because under these conditions the solution becomes opaque (independent of the presence of peptide), and over time $Ni_3(PO_4)_2$ falls out of solution.

The UV/visible spectra correspond quite well to those that were reported for the 12-mer maquette[22] and the reduced (Ni^{II}) form of the enzyme itself.[16] This, together with the facts that no ESR signal could be detected, and that NMR spectra of the nickel complex show no evidence of paramagnetic effects indicates that, in accord with Shearer and Long, only the Ni^{II} oxidation state is present in the biomimetic although both Ni^{II} and Ni^{III} states are present in the enzyme.[14]

Determination of the 3D solution structure

Standard 1D $^1H/^{13}C$ NMR spectra of the nonapeptide are very well resolved with unusually narrow line widths. Spectra do not change in the slightest upon addition of Ni^{II} in the form of $NiCl_2$ or $Ni(ClO_4)_2$. In addition, we observed an unusual thermostability from 25 to well above 60 °C; we interpret these facts as being indicative for the presence of a single predetermined 3D conformation with a preformed cavity for nickel binding. Due to the well-resolved spectra, complete assignments as well as extensive standard 2D NMR spectroscopic experiments

could be performed. Representative 1D and 2D spectra can be found in the Supporting Information.

All ^{1}H,^{1}H ROESY H$^\alpha$ resonances that are needed for a sequential walk analysis of the backbone structure could be identified with the sole exception of Asp3, which was covered by the water resonance and thus could only be detected in D_2O solvent. The H^{N}H$^\alpha$ region of this spectrum is illustrated in Figure 2. Analysis of the ^{1}H,^{1}H ROESY spectra allowed a total of

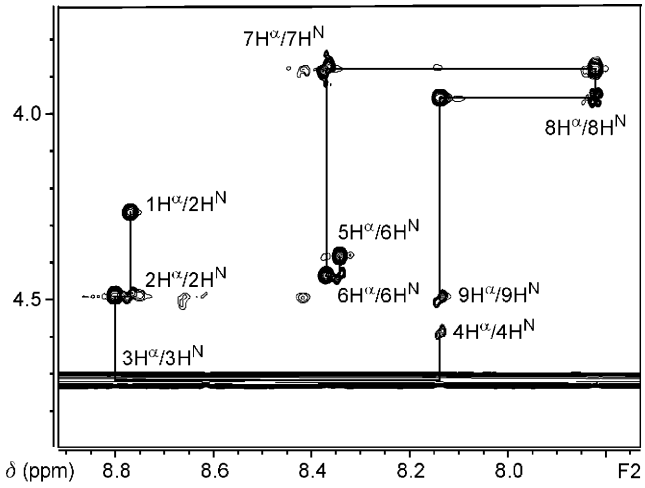

Figure 2. H^{N}H$^\alpha$ region of the ^{1}H,^{1}H ROESY spectrum of the nonapeptide showing the sequential walk.

31 experimental NOE (nuclear Overhauser enhancement) distance constraints (Table S1) to be identified and classified as being strong ($<$2.8 Å), medium ($<$3.6 Å) and weak ($<$5.5 Å).

No differences in the NOE pattern were observed when comparing NMR spectra that were obtained in the presence and the absence of Ni^{II} ions. As was expected, most of the NOE signals resulted from protons of one amino acid interacting with protons from neighboring residues. However, several crosspeaks clearly indicate the presence of a macrocylic ring conformation, especially a $H^{\delta2}_{His1>}$–H^{N}_{Tyr9} and two $H^{\beta2/\beta3}_{Cys2}$–H^{N}_{Leu4} signals. These experimental NOE constraints formed the basis of a local conformational analysis that allowed 39 torsion angle constraints, and further defined 25 torsion angles to be assigned to the nonapeptide (and its nickel complex). These provided the basis for the generation of 3D structures by using the torsion–angle dynamics program CYANA.[24] Several ensembles of related structures that did not violate the distance and dihedral restraints more than $\pm$0.2 Å and $\pm5^\circ$ were found. All ensembles had a general ring structure in common, in which the nonapeptide had more or less folded in upon itself. This characteristic allowed us to immediately reject most of the ensembles due to the fact that closer inspection revealed that these conformations would result in additional ROESY crosspeaks, which were not experimentally observed. Because the spectra are basically identical whether or not Ni^{II} is present, we also considered the possibility that a family of nonapeptide conformations exists with a predetermined nickel-binding site (the additional constraints listed in the methods section). It is quite interesting that this last possibility, which produced the lowest target functions of all (structural statistics can be found in Table 1) did not emerge from initial investigations of the

Table 1. Structural statistics for the ensemble of the ten "best" (lowest target functions) conformations of the nonapeptide.

Distance and dihedral constraints	
distance constraints	31
nickel-binding position constraints	6
total dihedral angle restraints	39
statistics for the ten "best" conformations	
violations	Mean (s.d.)
target function [Å^2]	0.349 (0.0032)
distance constraints [Å]	0.014 (0.0019)
max. distance constraint violation [Å]	0.078 (0.0042)
dihedral angle constraints [°]	0.011 (0.0112)
max. dihedral angle violation [°]	0.061 (0.0582)
mean global r.m.s.d. [Å]	
heavy atoms (residues 1–6)	0.94 (0.34)
backbone atoms (residues 1–6)	0.19 (0.14)

conformational manifold. The ensemble of the ten "best" conformations of the nonapeptide is illustrated in Figure 3.

This ensemble shows a good convergence into a single cyclic arrangement for the first six residues (His1 to Cys6) with

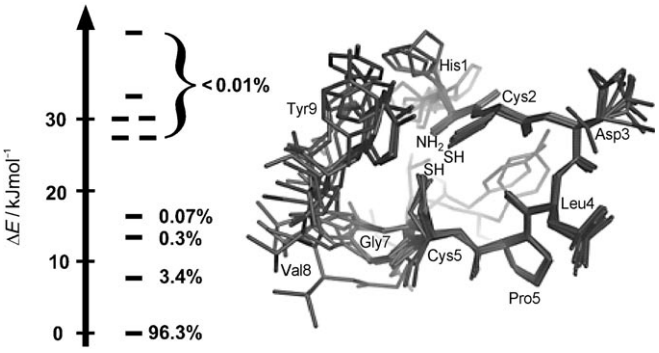

Figure 3. Left: The Boltzmann distributions (relative energies) of all ten conformers were calculated at the BP86(MARI-J;COSMO)/SV(P) level of theory. Right: Ensemble of ten conformations of the nonapeptide with the lowest target functions as obtained from CYANA.

thermal motion occurring only in the side chains of Asp3 and Leu4, which point away from the cyclic structure into the solvent. Participation of the carboxylate side chain of Asp3 in nickel binding can be ruled out due to its orientation. The imidazole ring in His1 also exhibits a certain degree of rotational freedom.

The nickel-coordinating side chain of Cys6 exhibits two different conformational possibilities as represented by χ^1_6 torsion angles of $+66^\circ$ and -91° (mean values). However, the location of the sulfur atom that is needed for nickel coordination remains invariant due to compensation by the χ^2_6 torsion angle. The conformational situation is much less well defined for the three C-terminal residues Gly7 to Tyr9. We attribute this to a

greater degree of dynamic freedom, which allows for a certain degree of motional disorder in a conic region that originates at the peptide linkage between Cys6-Gly7 and progressively continuing down the three C-terminal residues. Due to this disorder, interactions of the aromatic ring (Tyr9) with the well-defined nickel-binding region could not be detected in any of the NMR spectra. However, regardless of the degree of motional freedom present, the experimentally observed $H^{\delta 2}_{His1}$–H^{N}_{Tyr9} NOE crosspeak definitely places the phenol ring of Tyr9 in the neighborhood of the imidazole ring in His1.

All ten structures were further refined by full optimizations, which were carried out at the BP86(MARI-J;COSMO)/SV(P) level of theory. Bulk solvent effects (water) were explicitly taken into account during the optimizations by using the COSMO approximation. All conformations are stationary points on the BP86 hypersurface. Figure 3 contains an approximation of the conformational distribution at 25 °C that were calculated by using the relative energies and a simple statistical Boltzmann distribution. It is quite interesting that only four of the possible conformations can be expected to be populated to a large extent in solution. We then refined these four conformations by reoptimizing them at the BP86(MARI-J;COSMO)/def2-TZVP level of theory. It is significant that all four conformations have the same 3D His1-Cys6 backbone structure (Figure 4). Even in the absence of Ni^{II}, the nonapeptide spontaneously folds into a macrocyclic conformation with four ligands optimally oriented for nickel binding (the two thiol groups of Cys2/6, the N-terminal amino group and the amide nitrogen atom in the His1-Cys2 linkage). The conformers differ mainly in the relative positions of His1 and Tyr9, and in the conformation of the flexible Gy7-Val8-Tyr9 backbone.

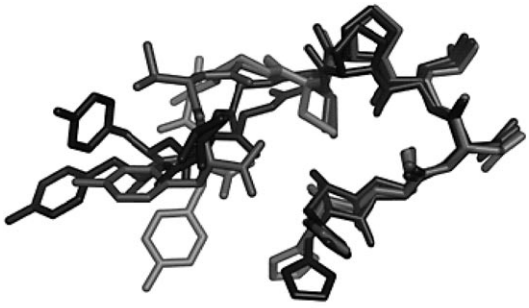

Conformer	P1	P2	P3	P4
ΔE_{rel}	0.0	8.9	20.5	24.9

Figure 4. The four most preferred conformations of the nonapeptide and their relative energies (kJ mol^{-1}) as obtained by BP86-D(RI;COSMO)/def2-TZVP//BP86(MARI-J;COSMO)/def2-TZVP calculations; the global minimum is the structure in light gray.

Interactions between aromatic side chains in biological macromolecules (here His1 and Tyr9) are known to be significantly influenced by van der Waals forces (noncovalent interactions)[25]—an effect that has not been included in the calculations presented here. Indeed, DFT methods possess the general disadvantage that they cannot describe the long-range electron correlations that are responsible for these dispersion forces.[26] Recent work by Grimme et al. has, however, provided a means of partially overcoming this deficit by using a correction that is based on damped long-range potentials (the DFT-D method).[27] We have included these "weak" interactions in this study by means of single-point calculations at the BP86-D-(RI;COSMO)/def-TZVP level on the four conformations that were refined at the BP86(MARI-J;COSMO)/def2-TZVP level. At this level, the two conformations with the highest energies can be excluded. The energy gap between the two lowest conformations (8.9 kJ mol^{-1}) is still too small to assign a single 3D conformation as the preferred solution structure. However, the extremely high structural similarity between these two conformations definitely explains the very well-resolved experimental spectra.

Conformation of the proline 5 peptide linkage

One of the more interesting structural features is the fact that Pro5 exhibits a *trans* peptide bond as could be conclusively verified from the presence of sets of H^{α}_{i-1} to H^{δ} cross peaks in $^1H,^1H$ ROESY spectra (Figure 5). No evidence for a *cis* conformation is present in any of the spectra. In direct contrast to this, the crystallographic structures of both variants of NiSOD exhibit a *cis* linkage for Pro5.[14,15] The energy difference between the *cis* and *trans* conformations of proline is generally quite low and it is a well-known fact that *cis–trans* isomerization in proline linkages is often one of the rate-determining steps in protein folding.[28] Interactions between neighboring groups (H-bridges, etc.) often determine which conformation *cis*/*trans* is preferred.[29]

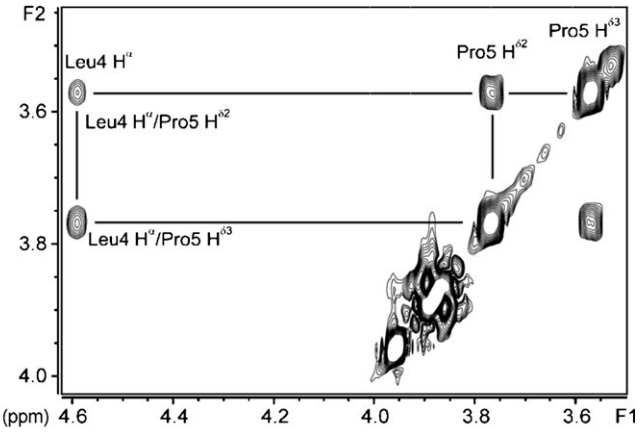

Figure 5. Zoomed region of the $^1H,^1H$ ROESY spectrum of the nonapeptide showing the H^{α}_{i-1}-to-H^{δ}_{i} cross signals that are typical for a *trans* proline linkage.

In order to directly compare the structure of the nonapeptide to the structure of the enzyme, we took the solid-state coordinates of the "nickel hook" (PDB ID: 1Q0M, ref. [15]), removed the Ni^{II} ion, and refined the structure by optimizing it at the BP86(MARI-J;COSMO)/def2-TZVP level of theory. The

resulting structure is overlaid on the 3D solution structure of the first six residues of the nonapeptide in Figure 6.

It is most intriguing that the conformation (*cis*/*trans*) of Pro5 has no significant influence on the positions of the four heteroatoms that are needed to coordinate the Ni^{II} ion (circled in Figure 6), which remain surprisingly more or less invariant. The only significant conformational change is the relative position of the Asp3 linkage which appears to be "pushed to the back" in the *cis* conformation. We attribute the observed *trans* preference of the solution structure exclusively to the backbone folding of the first six amino acids (His1-Cys6). In the belief that this differential stability is due to intramolecular hydrogen bonding interactions (a factor that is known to affect the proline conformation[29]), we then investigated the hydrogen-bond network in both models by using the shared-electron number (SEN) method.[30,31]

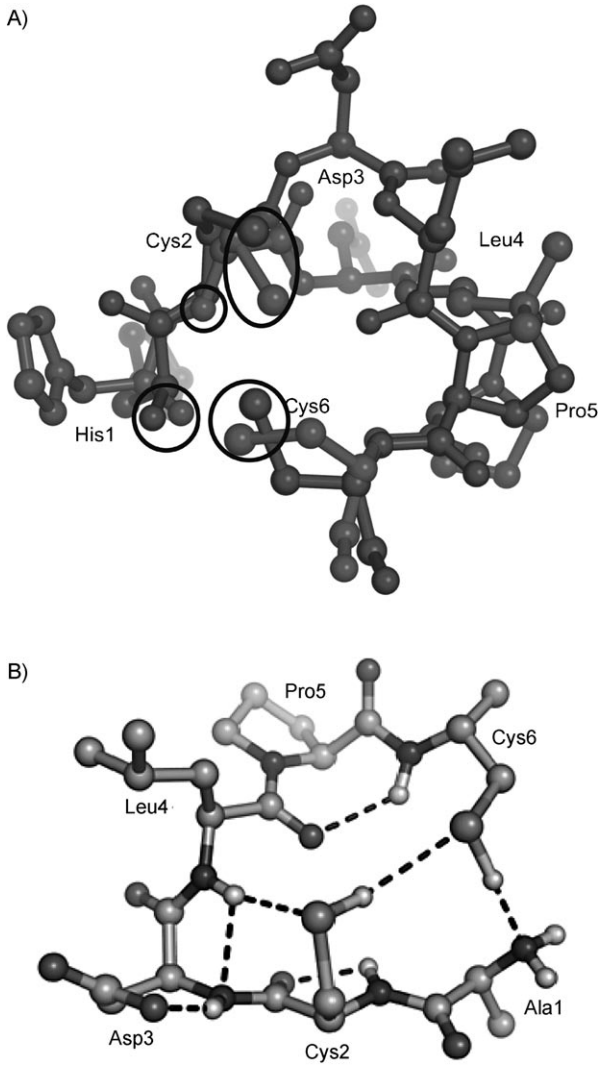

Figure 6. A) 3D solution structure of the first six residues in the nonapeptide overlaid on the solid state structure of NiSOD (PDB ID: 1Q0M). B) Intramolecular hydrogen bond network stabilizing the macrocyclic structure of the nonapeptide. All calculations were performed at the BP86(MARI-J;COSMO)/def2-TZVP level of theory.

In the SEN approach, the energy of a specific hydrogen bond, E_{HB} can be approximated by multiplying an empirical factor λ with the shared-electron number σ that was obtained by an orbital analysis [Eq. (4)]:

$$E_{HB} = \lambda\sigma \quad (4)$$

Before this analysis could be performed, it first proved necessary to calibrate the method because λ has not yet been determined for the def2-TZVP basis set. In addition, the test sets that were previously used to calibrate the method did not include typical hydrogen bonds found in peptides.[30,31] After developing a modified test set (Supporting Information), our investigations revealed that it is necessary to subdivide the hydrogen bonds that occur in peptide chains into two subclasses. The first subclass contains all hydrogen bonds that do not involve sulfur as either the proton donor and/or as the proton acceptor. For this subclass, the two-center shared-electron number (σ_{HA}) can be employed, as has been previously described.[30,31] Due to the high polarizability of sulfur, it proved necessary to include longer-range effects in the correlation (the H-bond is no longer "localized" between two centers). We found that use of the three-center shared-electron (σ_{DHA}) number is necessary for a proper description of hydrogen bonds involving sulfur. By using this approach with the def2-TZVP basis set, we determined the empirical factor λ to be $+195\ kJ\,mol^{-1}$ for sulfur-containing and $-391\ kJ\,mol^{-1}$ for non-sulfur-containing hydrogen bonds, respectively.

SEN analyses of the model structures illustrated in Figure 6 revealed the presence of seven intramolecular hydrogen bonds in the *trans* conformation, and only five in the *cis* conformation. This hydrogen-bond network stabilizes the *trans* conformation by $90.7\ kJ\,mol^{-1}$, whereas the *cis* conformation is stabilized by only $44.6\ kJ\,mol^{-1}$; this leads to a relative *trans* stabilization ($\Delta E_{cis/trans}$) of $46.1\ kJ\,mol^{-1}$. This is nearly the same as the total energy difference between the solution (*trans*) and the solid-state conformation (*cis*) [$\Delta E_{total} = 46.5\ kJ\,mol^{-1}$], and confirms that the preference for the *trans* conformation in solution can indeed be attributed solely to the presence of this intramolecular hydrogen-bond network.

We then went on to analyze why the *cis* conformation is preferred in the solid state and discovered that this is also due to hydrogen bonding. We enlarged our model to include hydrogen-bonding interactions of the "nickel hook" with amino acid side chains of residues in the second coordination sphere (which are absent in Figure 6). To do this, we again started from the protein databank coordinates of the solid state structure of NiSOD, fixed the positions of selected atoms to hold the model together and refined (reoptimized) it at the BP86-(MARI-J)/def2-TZVP level of theory. The pertinent second-sphere hydrogen-bonding interactions are illustrated in Figure 7. A SEN analysis of these second-sphere interactions revealed that they provide $137.7\ kJ\,mol^{-1}$ of stabilization energy. The largest contribution ($106.2\ kJ\,mol^{-1}$) is provided by strong hydrogen bonds of the charged Asp3 side chain with three

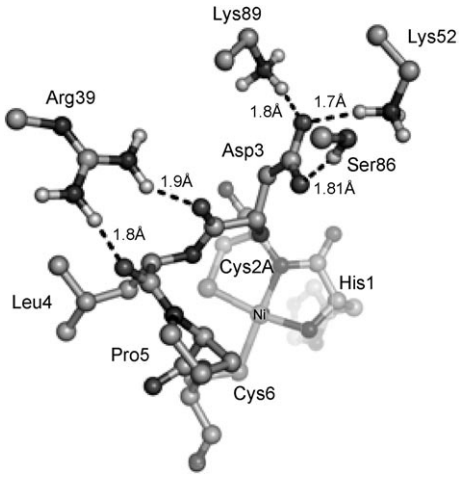

Figure 7. Hydrogen-bond network between the nickel hook and second-sphere residues in the solid-state structure of NiSOD (PDB ID: 1Q0M; coordinates refined at the BP86(MARI-J)/def2-TZVP level of theory).

second-sphere neighbors (Lys52, Ser86, Lys89). These interactions indirectly help determine the conformation of Pro5 by inducing a distortion of the backbone structure (Figure 7).

In addition to this, there are strong, specific interactions of two backbone carbonyl groups (Asp3Leu4 and Leu4Pro5) with Arg39 that directly stabilize the *cis* conformation of Pro5 by a total of 31.5 kJ mol^{-1}; this is almost enough in itself to overcome the intrinsic *trans* preference that is provided by the hook structure. These results reveal why Arg39 is an indispensible amino acid: mutation of this residue to Ala has been reported to completely destroy the enzymatic activity.[15] Our calculations indicate that this mutation might trigger a Pro5(*cis* → *trans*) conformational change, which would bring the carbonyl group in the Leu4-Pro5 backbone in a position in which it would block the nickel coordination site that is necessary for $O_2^{\bullet-}$ docking (discussed below).

Structure of the Ni^{II}–nonapeptide complex

According to ESI-MS experiments, the molecular weight of the Ni^{II}–nonapeptide complex formed upon addition of Ni^{II} to solutions of the nonapeptide is 1061.3 g mol^{-1}, which corresponds to the calculated weight of a [1:1] complex in which both thiol side chains have been deprotonated to provide ligands for Ni^{II}. The preformed nickel-binding site allowed us to simply remove the thiol protons of both cysteine side chains and place a Ni^{II} ion in the middle of the binding site as a starting point for DFT investigations. Subsequent optimization of both possible spin states ($S=0$, $S=2$) for the central Ni^{II} ion at the BP86(MARI-J;COSMO)/def2-TZVP level of theory resulted in two different possibilities for a [1:1] complex (Figure 8).

At this level of theory, the low-spin state is 69.8 kJ mol^{-1} more stable than the high-spin state. This preference for the

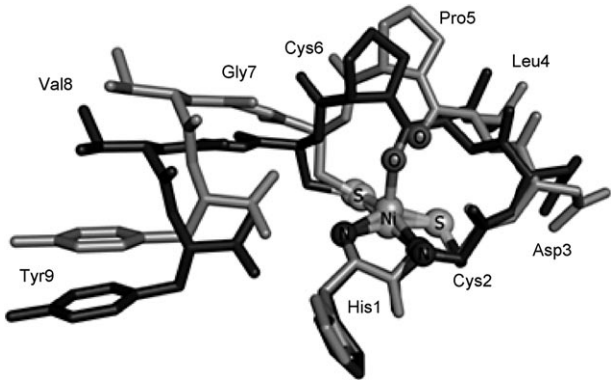

Figure 8. Comparison of the low spin (light gray) and high-spin state (dark gray) of the Ni^{II}–nonapeptide complex. The steric hindrance that prevents the approach of $O_2^{\bullet-}$ from the Pro5 side is obvious. Calculated at the BP86(MARI-J;COSMO)/def2-TZVP level of theory.

low-spin state is not unexpected because Reiher et al. have shown that the DFT spin-state calculations exhibit a method dependency on the exact exchange contribution of the functional employed, which, in the case of the BP86 functional, leads to a calculated overstabilization of the low-spin state.[32] Recent work by Zein et al.[33] has allowed us to select a reference geometry (illustrated in the Supporting Information) for determining a correction for the adiabatic energy gap $\Delta E_{high-low}$. At the BP86/def2-TZVP level of theory, the energy gap that was calculated for the reference structure was 101.6 kJ mol^{-1}, and at the B3LYP*/def2-TZVP level it was 69.3 kJ mol^{-1}; this demonstrates that the BP86 functional overestimates the stability of the low-spin state by approximately 32.3 kJ mol^{-1}. By applying this correction to our results, we predict the $\Delta E_{high-low}$ adiabatic spin-state gap for the biomimetic to be 37.5 kJ mol^{-1}. This corresponds quite well with the fact that a high-spin state could not be detected experimentally (ESR). However, this gap is not so large as to exclude the possibility that a high-spin state could be transiently accessed during a catalytic circle.

In the low-spin state, the metallocomplex exhibits the expected square planar geometry (Table 2). The high-spin state is square pyramidal and the fifth ligand is the carbonyl group of the Leu4-Pro5 backbone. The *trans* conformation of the Pro5 peptide linkage prevents His1 from providing the fifth ligand (imidazole side chain). In both spin states, this carbonyl group

Table 2. Multiplicity [M_S], spin expectation values $<\hat{S}^2>$ and nickel-ligand bond lengths [Å] in the two different spin states of the Ni^{II}-nonapeptide complex. Calculated at the BP86(MARI-J)/def2-TZVP level of theory.

M_S	$<\hat{S}^2>$	Ni-N_{His1}	Ni-N_{Cys2}	Ni-S_{Cys2}	Ni-S_{Cys6}	Ni-O_{bkbn}
1	0.00	1.994	2.010	2.174	2.179	3.414
3	2.01	2.154	2.667	2.246	2.290	2.093

is clearly close enough to the Ni^{II} ion to prevent $O_2^{\bullet-}$ from approaching from that side of the complex. In both structures that are available for NiSOD enzymes, this is the side on which the substrate channel for $O_2^{\bullet-}$ is located.[14,15]

In the biomimetic, $O_2^{\bullet-}$ is clearly forced to approach from the "wrong" (His1) side. A shared coordination of both the side chain of His1 as well as $O_2^{\bullet-}$ from one and the same side seems quite strange; this leads us to the assumption that His1 is not essential for the catalytic function of this biomimetic. This is in clear contrast to enzymatic mutation experiments which assign an essential function to His1.[12,15]

SOD activity of the Ni^{II}–nonapeptide complex

A qualitative test for SOD activity based on a *p*-nitroblue tetrazolium chloride (NBT)/riboflavin/TMEDA assay[34] indicates that the Ni^{II}–nonapeptide complex is behaving as a functional SOD catalyst (Supporting Information). The addition of small amounts of KO_2 to a solution of the Ni^{II}–nonapeptide complex destroys it within a short time. However, UV/visible monitoring at 458 nm (typical Ni^{II}–S_{cys} bond excitation)[35] shows that, completely analogously to the 12-mer maquette[22] of Shearer and Long, our system is capable of surviving 60–90 s in a solution that contains a large amount of free $O_2^{\bullet-}$ (Supporting Information).

In an attempt to quantify the activity under physiological conditions, we performed the McCord–Fridovich activity test (described in the Experimental Section). According to this test, solutions of both the free peptide and Ni^{II} ions are SOD-inactive. Activity measurements on the Ni^{II}–nonapeptide complex proved to be complicated due to the fact that the UV/visible titration experiments suggest that an equilibrium between free peptide and Ni^{II} -complex is present and/or that an additional Ni^{II}, which is easily lost coordinates loosely (probably to one of the side chains). It is possible that several species are present in solution, each of which can be expected to exhibit a different activity. We first investigated the effect of excess Ni^{II} on the activity by working under $O_2^{\bullet-}$-limited conditions in which we could fairly reliably determine the molar amount of nonapeptide in the sample. In this manner, we could determine a *lower limit* to the activity of our biomimetic. A [1:1] Ni^{2+}/peptide ratio possesses an activity of about 830 U μmol^{-1} (Table 3). Increasing the relative amount of Ni^{II} to [2:1] increases the activity to 1250 U μmol^{-1}, which then is unaffected by a further increase in the molar amount of Ni^{II} (Supporting Information). To obtain an (estimated) upper limit for the activity, we then prepared a [2:1] Ni^{2+}/nonapeptide sample, which we then increasingly diluted to extrapolate to zero concentration (where free nonapeptide and not $O_2^{\bullet-}$ becomes the limiting factor). The activity rises exponentially to an upper limit of about 2100 U μmol^{-1}.

As a comparison, we report the enzymatic activity of the NiSOD that we recently isolated from *Streptomyces acidiscabies* E13 to be 75 000 U μmol^{-1} per subunit, which is a full order of magnitude larger. The rather "poor" performance of the biomimetic is most likely due to a change (His→backbone carbonyl) in the fifth ligand, which is necessary for stabilizing a Ni^{III} species in the catalytic turnover. We suspect that this leads to a much poorer redox potential match with $O_2^{\bullet-}$ because the redox potential of a Ni^{II}→Ni^{III} transition is known to be quite sensitive to the ligand environment.[36]

Table 3. Estimated lower and upper limits of the activity [reported in U μmol^{-1}] of our biomimetic as compared to NiSODs isolated from *S. coelicolor* and *S. acidiscabies* E13.

Ni^{II}/P[a]	Activity[b]	Activity[c]	Enzyme	Activity
1:1	830	–	*S. acidiscabies* E13	75 214[d]
2:1	1250	~2100	*S. coelicolor*	45 292[e]

[a] ratio of Ni^{II} ions to peptide (P). [b] Activity [U μmol^{-1}] measured under $O_2^{\bullet-}$ limited conditions (lower limit to the activity). [c] Activity [U μmol^{-1}] nonapeptide extrapolated to nonapeptide-limiting conditions (estimated upper limit to the activity). [d] U μmol^{-1} per subunit. [e] Ref. [7c]: 3380 U mg^{-1} per enzyme converted into U μmol^{-1} per subunit).

Search for a minimal functional motif

The results above indicate that the imidazole side chain in His1 might not be essential for the functionality of the biomimetic. We therefore synthesized a nonapeptide mutant in which His1 was replaced with Ala. Subsequent activity measurements showed a very slight decrease in the activity, which, however, is well within the error of the method that was employed (Figure 9); this confirms that the imidazole ring is indeed non-

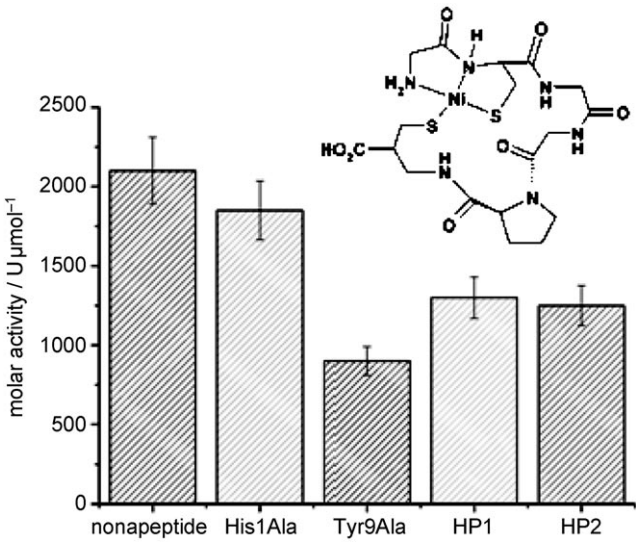

Figure 9. SOD activity (U μmol^{-1}) of aqueous solutions of several peptide modifications in the presence of Ni^{II} ions and the structure of a minimal peptide-based functional motif for SOD catalysis. Nonapeptide: HCALPCGVY-NH_2, His^1Ala: ACALPCGVY-NH_2, Tyr9Ala: ACALPCGVA-NH_2, HP1: ACDAPC-NH_2, HP2: ACAAPC-NH_2.

essential. In the enzyme, His1 provides a fifth ligand for the nickel ion, which easily cycles between diamagnetic Ni^{II} and paramagenetic Ni^{III} states. One of the two available solid state structures of NiSODs revealed the presence of Ni^{III}, and the

second contained a mixture of Ni^{II} and Ni^{III} states.[14,15] It is quite interesting that selected mutation (His1→Ala) in the enzyme not only destroyed the catalytic activity[15] but also changed the preference for the oxidation state of nickel, which in the mutant is now diamagnetic Ni^{II}.[12] This corresponds quite well with the fact that an ESR signal for Ni^{III} could not be detected in solutions of the biomimetic. We postulate that the *trans* conformation of Pro5 is responsible for this change in oxidation state preference because the central nickel ion is now forced to employ a carbonyl group as the fifth ligand. We are now attempting to enforce a *cis* conformation (replacement of Pro5 with modified cyclopentane rings). We expect that His1 will again prove to be essential; a Ni^{III} state should be present and the catalytic activity will probably dramatically rise.

Further structure–function investigations on the biomimetic shows that a ring system in the position of Pro5 is essential because this introduces the necessary "turn" in the peptide chain for both generating the prefolded macrocyclic structure and maintaining conformational stability. Mutation of Pro5 to Ala has drastic consequences. Upon removing the newly synthesized nonapeptide from the resin, it promptly polymerizes to form a white, insoluble polymer that cannot be further characterized.

Selected mutation (Tyr9→Ala) in the enzyme destroys the catalytic activity[15] and it has been postulated that Tyr9 could be responsible for intercepting and properly positioning $O_2^{\bullet-}$.[14] Mutation of Tyr9 to Ala in the biomimetic indicates that Tyr9 definitely plays an ancillary role in the mode of action, because the measured activity of the mutant peptide drops by a factor of two. This residue cannot be considered to be "essential" however, because the mutant is still capable of catalytically disproportionating $O_2^{\bullet-}$. The flexibility of the last three residues then prompted us to see if they could be dispensed with. Neglecting the last three amino acids (Gly7-Val8-Tyr9; HP1 and HP2 in Figure 9) increases the activity as compared to the Tyr9Ala mutant. In the absence of Tyr9, the last three residues obviously have an inhibitor character.

Because we suspected that the side chains of Asp3 and Leu4 are also nonessential, we prepared two hexapeptides ACDAPC-NH_2 (Leu4→Ala; HP1 in Figure 9) and ACAAPC-NH_2 (HP2) and complexed them with nickel ions. Both are functional biomimetica, albeit slightly less active than the original nonapeptide. It is not surprising that Leu4 is a nonessential amino acid; it is not strictly conserved in many NiSODs, however, Asp3 is.[15] As discussed above, we attribute this to be due to second-sphere interactions that are necessary to stabilize a *cis* Pro5 conformation and not to an essential catalytic function. The minimal peptide-based functional motif for SOD catalysis identified by these experiments is illustrated in Figure 9.

Conclusions

The first nine amino acids (the so-called "nickel hook") in the sequence of NiSODs provide a functional SOD biomimetic when complexed with nickel ions. In contrast to enzymatic systems in which a Ni^{II}→Ni^{III} equilibrium is present, the biomimetic possesses a diamagnetic Ni^{II} ground state. The 3D solution structure shows that the first six residues provide a prefolded, macrocyclic ligand environment that is optimally structured for complexation with Ni^{II}. Thermal motion (conformational flexibility) occurs only in the last three residues (Gly7-Val8-Tyr9) and side chains (Asp3, Leu4), which point out and away from the macrocyclic center. In contrast to the structures of NiSOD enzymes, the biomimetic exhibits a *trans* peptide Pro5 bond. A detailed analysis showed that this *trans* preference of the solution structure is due exclusively to the presence of an extended *intra*molecular hydrogen-bond network that is generated by the backbone folding of the first six amino acids. The *cis* preference found in NiSOD enzymes is also due to the presence of a stabilizing hydrogen-bond network: an *inter*molecular one this time with specific second-sphere interactions of the "nickel hook" with amino acid side chains of residues further away from the active site (specifically Arg39).

The *trans* conformation of Pro5 prevents His1 from providing the fifth ligand necessary for stabilizing a Ni^{III} oxidation state. Modification of the peptide sequence confirmed that the imidazole side chain of His1 is indeed nonessential for the function of the biomimetic. DFT calculations indicate that the carbonyl group in the Pro5-Leu4 peptide bond probably assumes the role of the fifth ligand. We attribute the relatively poor catalytic performance of the biomimetic (as compared to enzymatic systems) to this ligand exchange, which probably induces a poor redox potential match with $O_2^{\bullet-}$. We postulate that upon enforcing a *cis* conformation in Pro5, His1 will again prove essential: a Ni^{III} state will be stabilized, and the catalytic activity will dramatically rise. Further structure–function investigations allowed a functional minimal motif that contains only six amino acid residues (ACAAPC-NH_2) to be identified. These investigations demonstrate conclusively that a substructure of the "nickel hook" is clearly capable of catalytically disproportionating $O_2^{\bullet-}$, thus providing direct experimental evidence for the presence of a fundamental "inner-sphere" mechanism for NiSODs in general.

Experimental Section

Peptide syntheses: Standard Fmoc coupling procedures (details available in the Supporting Information) were used to synthesize the nonapeptide hook sequence HCDLPCGVY-NH_2 (*S. coelicolor*) in acceptable yields (90% crude; 60% HPLC pure). By using the same general procedure, the following nonapeptide mutants were obtained in similar yields: ACDLPCGVT-NH_2 (His1→Ala), HCDLPCGVA-NH_2 (Tyr9→Ala). Alanine substitution of Pro5 (HCDLACGVA-NH_2) proved problematical. The synthesis was successful; however this mutation immediately cross-polymerized (intermolecular disulfide bridges) upon removal from the resin to form an insoluble white powder that was not further characterized. For further mechanistic investigations, the following hexapeptide sequences were also synthesized in yields of 60–80% HPLC-pure: ACDAPC-NH_2 (His1, Leu4→Ala), ACDAPC-NH_2 (His1, Leu4→Ala), and ACAAPC-NH_2 (His1, Asp3, Leu4→Ala). The peptide sequences were confirmed by ESI-mass spectroscopy and quantitative ASA as described in the Supporting Information. All of these synthetic peptides tend to irreversibly collect TFA salts (present upon HPLC purification) that cannot be removed by freeze drying (lyophilization). The amount of peptide that was actually present in solid state probes thus

varied between 50 and 85%. All activity measurements contained a mass correction that was obtained from ASA analyses. Probes were stored in the solid state at −25 °C. An protective atmosphere of argon proved to be unnecessary.

Qualitative SOD assay: Principle: A steady state concentration of $O^{\bullet 2-}$ radicals was generated with riboflavin/TMEDA. These react with nitroblue tetrazolium (NBT), which turned dark blue, almost black. If a species with SOD activity were present, the $O^{\bullet 2-}$ radicals were disposed of before they reacted with NBT (solution remains colorless).[35] Standard solutions: NBT (2 mg in 1 mL H_2O dest.); riboflavin/TMEDA (2.6 mg riboflavin, 1.0 mL TMEDA in 250 mL 50 mM 0.1 M potassium phosphate buffer pH 7.8). For the assay, H_2O dest. (500 μL), nonapeptide (0.2 mg), and 2 mM $NiCl_2$ (500 μL) were mixed at RT. In the control solutions, nonapeptide or the nickel salt or both were replaced with H_2O (dest). NBT solution (100 μL) was added to all four probes. After 15 min's incubation in the dark, the reaction was initiated by placing the probes on a light table or scanner.

Quantitative measurement of SOD activity: Measurements were performed according to the McCord/Friedovich method.[37] Principle: Xanthine oxidase oxidized xanthine to generate $O_2^{\bullet -}$ at a low and constant (steady state) rate. Free $O_2^{\bullet -}$ then reduces NBT, which could be monitored photometrically at 560 nm. If an added substance was SOD-active, it competed for $O_2^{\bullet -}$, thus inhibiting the reduction of NBT. The measured rise in the extinction slope was lower than the control reaction. The SOD-activity was defined as the half-limited reduction of NBT and measured by a reduction in the slope (the linear phase was used) and set relative to the concentration of the substance: $U = 2(A_{control} - A_{substance})/A_{control}$ where U is the activity of the substance relative to the amount in the probe (usually given in U mg^{-1} or U μmol^{-1}).

Standard solutions: xanthine oxidase (40 U/4.2 mL; 80 μL enzyme solution in 9.0 μL 50 mM potassium phosphate buffer pH 7.8 solution freshly prepared), xanthine (3 mg dissolved in three drops of 1 M NaOH then adjusted to pH 7.8 in 25 mL of 50 mM potassium phosphate buffer), NBT (1.5 mg in 1 mL 50 mM phosphate buffer pH 7.8). Control: 50 mM potassium phosphate buffer pH 7.8 (1.0 mL), xanthine standard (100 μL) and xanthine oxidase standard (250 μL) were added to a cuvette (plastic, halfmicro). The cuvette was shaken and measurements performed immediately. A sample (100 μL) of the above buffer solution was replaced with a 50 mM phosphate buffer pH 7.8 solution (100 μL) that contained the probe in the desired concentration. Because the nonapeptide was hydroscopic and tended to collect salts (TFA), all samples were carefully dried before measurement, and a mass correction, which was obtained by ASA analyses was included in the activity determinations. All measurements were performed in triplicate.

Enzymatic activity of the NiSOD from *S. acidiscabies* E13: The enzyme was purified to apparent homogeneity from cells that were grown in a 0.2 mM nickel-containing minimal medium by essentially following literature protocol.[7c] After ammonium sulfate fractionation, anion exchange chromatography, gel filtration and a second anion exchange chromatography were applied. Quantitative determination of the enzymatic activity was performed as described above.

NMR spectroscopy: Standard 1D spectra were taken on an Avance 400 instrument (Bruker) with a ^1H resonance frequency of 400.2 MHz and a ^{13}C resonance frequency of 100.6 MHz. Standard 2D NMR[38] spectra were acquired on Varian UNITY *INOVA* 600 MHz and 750 MHz spectrometers at 298 K. Samples were dissolved either in 90% H_2O/10% D_2O or 99.9% D_2O without any added buffer. Solutions typically exhibited pH values between 5 and 6. The protein concentrations were in the 0.1–0.2 mM range. Probes of the nickel complex were generated by adding 3 equiv of $Ni(ClO_4)_2$ or $NiCl_2$ to an NMR tube that contained 0.1–0.2 mM nonapeptide in 90% H_2O/10% D_2O or 99.9% D_2O. For heteronuclear spectra, the gradient-selected sensitivity-enhanced mode was employed. Raw NMR spectroscopic data were processed by using the VNMR[39] program package. Directly and indirectly detected time domain data of the 2D spectra were processed by applying a 90° phase-shifted square sinebell. Data sets were zero-filled in each dimension prior to Fourier transformation. The program XEASY[40] was used for visualization and analysis of the spectra. All spectra that were obtained for the nickel complex were basically identical to those of the nonapeptide. Proton resonance assignments were made by using a combination of $^1H,^{13}C$ HMBC, $^1H,^{13}C$ HSQC-TOCSY, $^1H,^1H$ COSY, $^1H,^1H$ TOCSY (40 ms spinlock time) and $^1H,^1H$ ROESY ($\tau_m = 50$, 150 and 200 ms) experiments. Distance constraints were taken from $^1H,^1H$ ROESY spectra and classified according to their intensities. An r^{-6} dependence of intensity on distance was assumed, and three categories were assigned: strong, medium and weak with upper bounds of 2.8, 3.6 and 5.5 Å, respectively. In the case of methyl groups (Val8) and equivalent aromatic ring protons (Tyr9), the appropriate pseudo-atom corrections were applied.

Initial conformational manifold: Locally restricted conformational analyses that were based on the experimental NOE distance constraints were performed by using the FOUND[41] module. The resulting torsion angle restrictions together with the NOE constraints were used as the basis for generating manifolds of potential structural families by using simulated annealing torsion angle dynamics as implemented in the CYANA[24] package. In initial structure calculations, 100 random nonapeptide conformers were generated and subjected to simulated annealing. In the case of the Ni^{II} –peptide complex, six additional upper and lower limit constraints of 1.90–2.10 Å which define a planar coordination environment for Ni^{II} that involved the S^{γ} atoms of Cys2 and Cys6 as well as the backbone nitrogen atoms of residues His1 and Cys2 were introduced. This further allowed the torsion angles of ψ_1, ϕ_2 and χ^1_2 to be constrained to values around 0°, −60° and 0°, respectively. From each structural family obtained, the 10 structures with the lowest CYANA target functions were selected to represent initial NMR spectroscopic solution structures.

DFT calculations: Most of the calculations were carried out by using the BP86[42] density functional together with the multipole-accelerated resolution of identity (MARI-J)[43] approximation using the TURBOMOLE[44] suite of programs. Full geometry optimizations were generally performed by using the def2-TZVP[45] basis set. Only the investigation of the conformational manifold of the nonapeptide employed the smaller SV(P)[46] basis set. Unless otherwise mentioned, solvent effects (water) were explicitly considered using the COSMO[47] solvation model. The qmpot-tool[48] was employed for Cartesian coordination fixation as needed. BP86(MARI-J;COSMO)/SV(P) energies provided the basis for a standard statistical thermodynamical evaluation (Boltzmann) of the conformational distribution.[49] Due to the size of the systems, frequency calculations were performed only on the two spin-states of the minimal biomimetic structure at the BP86(MARI-J)/def2-TZVP level of theory employing the SNF[50] program. The absence of negative eigenvalues shows that both spin states represented energy minima. The relative energy of the two spin states (adiabatic energy gap) was determined at the B3LYP*[32,51]/def2-TZVP level of theory. Recently, the importance of long range weak dispersion interactions in organic and bioorganic molecules has been demonstrated.[27] To consider

these interactions in our investigations, we performed single-point calculations by using the BP86-D[52] method as implemented in the ORCA[53] program package. Intramolecular hydrogen bond energies were determined by using the "two-center shared-electron number" (σ_{SEN}) method that was first proposed by Reiher.[30] Instead of employing the improvement that was proposed by Thar and Kirchner,[31] we performed a simpler division, which we believe is sufficient for describing hydrogen bonds in peptides. We partitioned the hydrogen bonds into two subclasses. One subclass contained sulfur as either the acceptor or donor atom. The second contained all other types of hydrogen bonds. We employed the three-center shared-electron number for describing the sulfur subclass and the two-center number for the second subclass.

Acknowledgements

Financial support by the Deutsche Forschungsgemeinschaft (Collaborative Research Center 436, Jena, Germany) and the Thüringer Ministerium für Wissenschaft, Forschung und Kunst (Erfurt, Germany) is gratefully acknowledged. The Fritz Lipmann Institute is financially supported by the State of Thuringia and the Federal Government of Germany. In conjunction with the SFB 436, we thank Prof. M. Reiher for helping make this project possible by providing computer resources. S.Z. expresses his gratitude for the generous allocation of computer time at the NIC Jülich.

Keywords: density functional calculations · nickel · NiSOD · protein modifications · superoxide dismutases

[1] See for example: D. C. Wallace, *Science* **1992**, *256*, 628.
[2] V. Cizewski Culotta, M. Yang, T. V. O'Halloran, *Biochim. Biophys. Acta Mol. Cell Res.* **2006**, *1763*, 747–758.
[3] See, for example: a) T. A. Jackson, E. Yikilmaz, A. F. Miller, T. C. Brunold, *J. Am. Chem. Soc.* **2003**, *125*, 8348–8363; b) C. A. Kerfeld, S. Yoshida, K. T. Tran, T. O. Yeates, D. Cascio, H. Bottin, C. Berthomieu, M. Sugiura, A. Boussac, *J. Biol. Inorg. Chem.* **2003**, *8*, 707–714 and references therein.
[4] See, for example: a) T. A. Jackson, T. C. Brunold, *Acc. Chem. Res.* **2004**, *37*, 461–470; b) M. S. Lah, M. M. Dixon, K. A. Pattridge, W. C. Stallings, J. A. Fee, M. L. Ludwig, *Biochemistry* **1995**, *34*, 1646–1660 and references therein.
[5] See for example: a) T. A. Jackson, A. Karapetian, A. F Miller, T. C. Brunold, *J. Am. Chem. Soc.* **2004**, *126*, 12477–12491; b) A. S. Hearn, M. E. Stroupe, D. E. Cabelli, C. A. Ramilo, J. P. Luba, J. A. Tainer, H. S. Nick, D. N. Silverman, *Biochemistry* **2003**, *42*, 2781–2789 and references therein.
[6] See for example: a) A. Amadei, M. D'Allesandro, M. Paci, A. Di Nola, M. Aschi, *J. Phys. Chem. B* **2006**, *110*, 7538–7544; b) V. Pelmenschikov, P. E. M. Siegbahn, *Inorg. Chem.* **2005**, *44*, 3311–3320; c) M. D'Alessandro, M. Aschi, M. Paci, A. Di Nola, A. Amadei, *J. Phys. Chem. B* **2004**, *108*, 16255–16260 and references therein.
[7] a) H. D. Youn, H. Youn, J. W. Lee, Y. I. Yim, J. K. Lee, Y. C. Hah, S. O. Kang, *Arch. Biochem. Biophys.* **1996**, *334*, 341–348; b) E. J. Kim, H. P. Kim, Y. C. Hah, J. H. Roe, *Eur. J. Biochem.* **1996**, *241*, 178–185; c) H. D. Youn, E. J. Kim, J. H. Roe, Y. C. Hah, S. O. Kang, *Biochem. J.* **1996**, *318*, 889–896.
[8] V. Leclere, P. Boiron, R. Blondeau, *Curr. Microbiol.* **1999**, *39*, 365–368.
[9] a) T. Eitinger, *J. Bacteriol.* **2004**, *186*, 7821–7825; b) B. Palenik, B. Brahamsha, F. W. Larimer, M. Land, L. Hauser, P. Chain, J. Lamerdin, W. Regala, E. E. Allen, J. McCarren, I. Paulsen, A. Dufresne, F. Partensky, E. A. Webb, J. Waterbury, *Nature* **2003**, *424*, 1037–1042; c) G. Rocap, F. W. Larimer, J. Lamerdin, S. Malfatti, P. Chain, N. A. Ahlgren, A. Arellano, M. Coleman, L. Hauser, W. R. Hess, Z. I. Johnson, M. Land, D. Lindell, A. F. Post, W. Regala, M. Shah, S. L. Shaw, C. Steglich, M. B. Sullivan, C. S. Ting, A. Tolonen, E. A. Webb, E. R. Zinser, S. W. Chisholm, *Nature* **2003**, *424*, 1042.
[10] a) A. Schmidt, A. Schmidt, G. Haferburg, E. Kothe, *J. Basic Microbiol.* **2007**, *47*, 56–62; b) M. J. Amoroso, D. Schubert, P. Mitscherlich, P. Schumann, E. Kothe, *J. Basic Microbiol.* **2000**, *40*, 295–301.
[11] a) S. B. Choudhury, J.-W. Lee, G. Davidson, Y.-I. Yim, K. Bose, M. L. Sharma, S.-O. Kang, D. E. Cabelli, M. J. Maroney, *Biochemistry* **1999**, *38*, 3744–3752; b) F. Wolfe-Simon, D. Grzebyk, O. Schofield, P. G. Falkowski, *J. Phycol.* **2005**, *41*, 453–465.
[12] P. A. Bryngelson, S. E: Arobo, J. L. Pinkham, D. E. Cabelli, M. J. Maroney, *J. Am. Chem. Soc.* **2004**, *126*, 460–461.
[13] R. K. Szilagyi, P. A. Bryngelson, M. J. Maroney, B. Hedman, K. O. Hodgson, E. I. Solomon, *J. Am. Chem. Soc.* **2004**, *126*, 3018–3019.
[14] D. P. Barondeau, C. J. Kassmann, K. Bruns, J. A. Tainer, E. D. Getzoff, *Biochemistry* **2004**, *43*, 8038–8047.
[15] J. Wuerges, J. W. Lee, Y. I. Yim, H. S. Yim, S. O. Kang, K. D. Carugo, *Proc. Natl. Acad. Sci. USA* **2004**, *101*, 8569–8574.
[16] A. T. Fiedler, P. A. Bryngelson, M. J. Maroney, T. C. Brunold, *J. Am. Chem. Soc.* **2005**, *127*, 5449–5462.
[17] J. Sines, S. Allison, A. Wierzbicki, J. A. McCammon, *J. Phys. Chem.* **1990**, *94*, 959–961.
[18] V. Pelmenschikov, P. E. M. Siegbahn, *J. Am. Chem. Soc.* **2006**, *128*, 7466–7475.
[19] R. Prabhakar, K. Morokuma, D. G. Musaev, *J. Comput. Chem.* **2006**, *27*, 1438–1145.
[20] C. S. Mullins, C. A. Grapperhaus, P. M. Kozlowski, *J. Biol. Inorg. Chem.* **2006**, *11*, 617–625.
[21] D. P. Barondeau, E. D. Getzoff, *Curr. Opin. Struct. Biol.* **2004**, *14*, 765–774.
[22] a) J. Shearer, L. M. Long, *Inorg. Chem.* **2006**, *45*, 2358–2360; b) K. P. Neupane, J. Shearer, *Inorg. Chem.* **2006**, *45*, 10552–10566.
[23] M. Zahedi, H. Bahrami, *Kinet. Catal.* **2004**, *45*, 351–358.
[24] T. Herrmann, P. Güntert, K. Wüthrich, *J. Mol. Biol.* **2002**, *319*, 209–227.
[25] a) S. Bommarito, N. Peyret, J. SantaLucia Jr. , *Nuc. Acids Res.* **2000**, *28*, 1929–1934; b) D. H. Mathews, J. Sabina, M. Zuker, D. H. Turner, *J. Mol. Biol.* **1999**, *288*, 911–940.
[26] a) J. M. Pérez-Jordá, A. D. Becke, *Chem. Phys. Lett.* **1995**, *233*, 134–137; b) P. Hobza, J. Sponer, T. Reschel, *J. Comput. Chem.* **1995**, *16*, 1315–1325; c) S. Kristyán, P. Pulay, *Chem. Phys. Lett.* **1994**, *229*, 175–180.
[27] S. Grimme, J. Antony, T. Schwabe, C. Mück-Lichtenfeld, *Org. Biomol. Chem.* **2007**, *5*, 741–758.
[28] J. F. Brandts, H. R. Halvorson, M. Brennan, *Biochemistry* **1975**, *14*, 4953–4963.
[29] W. J. Wedemeyer, E. Welker, H. A. Scheraga, *Biochemistry* **2002**, *41*, 14637–14644.
[30] M. Reiher, D. Sellmann, B. A. Hess, *Theor. Chem. Acc.* **2001**, *106*, 379–392.
[31] J. Thar, B. Kirchner, *J. Phys. Chem. A* **2006**, *110*, 4229–4237.
[32] M. Reiher, O. Salomon, B. A: Hess, *Theor. Chem. Acc.* **2001**, *107*, 48–55.
[33] S. Zein, S. A. Borshch, P. Fleurat-Lessard, M. E. Casida, H. Chermette, *J. Chem. Phys.* **2007**, *126*, 014105.
[34] a) E. J. Kim, H. J. Chung, B. Suh, Y. C. Hah, J. H. Roe, *J. Bacteriol.* **1998**, *180*, 2014–2020; b) C. Beauchamp, I. Fridovich, *Anal. Biochem.* **1971**, *44*, 276–287.
[35] G. L. Ellman, *Arch. Biochem. Biophys.* **1959**, *82*, 70–77.
[36] a) J. Shearer, N. Zhao, *Inorg. Chem.* **2006**, *45*, 9637–9639; b) J. Hanss, H. J. Krüger, *Angew. Chem.* **1998**, *110*, 366–369; *Angew. Chem. Int. Ed.* **1998**, *37*, 360–363.
[37] a) D. P. Riley, *Chem. Rev.* **1999**, *99*, 2573–2587; b) R. H. Weiss, A. G. Flickinger, W. J. Rivers, M. M. Hardy, K. W. Aston, U. S. Ryan, D. P. Riley, *J. Biol. Chem.* **1993**, *268*, 23049–23054; c) J. M. McCord, I. Fridovich, *J. Biol. Chem.* **1969**, *244*, 6049–6055.
[38] K. Wüthrich, *NMR of Proteins and Nucleic Acids*, Wiley, New York, **1986**.
[39] Varian Inc., Palo Alto, USA; http://www.varianinc.com/cgi-bin/nav?products/nmr/software/vnmrj.
[40] C. Bartels, T. Xia, M. Billeter, P. Güntert, K. Wüthrich, *J Biomol. NMR* **1995**, *6*, 1–10.
[41] P. Güntert, M. Billeter, O. Ohlenschläger, L. R. Brown, K. Wüthrich, *J. Biomol. NMR* **1998**, *12*, 543–548.
[42] a) A. D. Becke, *Phys. Rev. A* **1988**, *38*, 3098–30100; b) P. P. Perdew, *Phys. Rev. B* **1986**, *33*, 8822–8824.
[43] a) F. Weigend, *Phys. Chem. Chem. Phys.* **2006**, *8*, 1057; b) M. Sierka, A. Hogekamp, R. Ahlrichs, *J. Chem. Phys.* **2003**, *118*, 9136; c) K. Eichkorn, F. Weigend, O. Treutler, R. Ahlrichs, *Theor. Chem. Acc.* **1997**, *97*, 119; d) K.

Eichkorn, O. Treutler, H. Öhm, M. Häser, R. Ahlrichs, *Chem. Phys. Lett.* **1995**, *240*, 283.
[44] R. Ahlrichs, M. Bär, M. Häser, H. Horn, C. Kölmel, *Chem. Phys. Lett.* **1989**, *162*, 165.
[45] F. Weigend, R. Ahlrichs, *Phys. Chem. Chem. Phys.* **2005**, *7*, 3297.
[46] A. Schäfer, H. Horn, R. Ahlrichs, *J. Chem. Phys.* **1992**, *97*, 2571.
[47] A. Schäfer A. Klamt, D. Sattel, J. C. W. Lohrenz, F. Eckert, *Phys. Chem. Chem. Phys.* **2000**, *2*, 2187.
[48] M. Sierka, J. Sauer, *J. Chem. Phys.* **2000**, *112*, 6983.
[49] D. A. McQuarrie, *Statistical Thermodynamics*, University Science Books, Mill Valley, **1973**.
[50] J. Neugebauer, M. Reiher, C. Kind, B. A. Hess, *J. Comput. Chem.* **2002**, *23*, 895.
[51] O. Salomon, M. Reiher, B. A. Hess, *J. Chem. Phys.* **2002**, *117*, 4729.
[52] a) S. Grimme, *J. Comput. Chem.* **2006**, *27*, 1787; b) J. Antony, S. Grimme, *Phys. Chem. Chem. Phys.* **2006**, *8*, 5287.
[53] Orca—an ab initio, DFT and semiempirical SCF-MO package: http://www.thch.uni-bonn.de/tc/orca.

Received: January 10, 2008
Published online on August 8, 2008

